Preparation of biomass-based porous carbon derived from waste ginger slices and its electrochemical performance

LI LIANGSHUO[a], QIN LIN[a], LI XINYU[b], DENG MING[c], FAN XIN[a]
[a]*Guangxi Key Laboratory of Optical and Electronic Materials and Devices, Key Laboratory of New Processing Technology for Nonferrous Metal & Materials of Ministry of Education, College of Materials Science & Engineering, Guilin University of Technology, Guilin 541004, China*
[b]*College of Science, Guilin University of Technology, Guilin 541004, PR China*
[c]*College of Information Science & Engineering, Guilin University of Technology, Guilin 541004, PR China*

As a new type of energy storage device, supercapacitor has attracted wide attentions due to its advantages such as short charging and discharging time, good cycle stability and higher power density. The main factor that affects the performance of supercapacitors is the electrode material, so electrode material with high specific capacitance has become one of the most focuses of current researches on supercapacitor. In this paper, biomass-based porous carbon material with high specific surface area was synthesized from ginger slices of food residue by activation and carbonization method. The prepared porous carbon was used as the electrode for supercapacitor, and the electrochemical performance was investigated. Its specific capacitance was as high as 227 F g^{-1} at the current density of 0.5 A g^{-1}, and it was assembled into an asymmetric supercapacitor with the voltage up to 1.6 V, and the maximum energy density was up to 13.65 Wh kg^{-1} at the power density of 399.5 W kg^{-1}, and the maximum power density was up to 7.99 kW kg^{-1} at the energy density of 9.1 Wh kg^{-1}. After 5,000 cycles at a current density of 5 A g^{-1}, the specific capacitance retention is 98.95 %.

(Received April 30, 2020; accepted November 25, 2020)

Keywords: Waste ginger slices, Biomass-based porous carbon, Characterization, Electrochemical performance

1. Introduction

With rapid development of science and technology, the demand for environment-friendly, efficient and sustainable energy storage equipment is increasing urgency [1-5]. As a new type of energy storage device, supercapacitor has the advantages such as high power density, fast charge/ discharge speed, good cycle stability and so on. It is well known that the electrode material is one of the main factors affecting the performance of supercapacitor. There are three main types of electrode materials for capacitors: carbon materials, transition metal compounds, and conductive polymers. Carbon materials mainly include activated carbon [6,7], carbon aerogels [8,9], graphite [10-12], carbon nanotubes [13-15], carbon fibers [16,17] and graphene [18-20]. Among them, activated carbon is widely used as electrode material in supercapacitor due to high porosity, high specific surface area and good charge accumulation at the electrolyte interface.

At the past decades, activated carbon is mostly prepared by activation method using coal, petroleum or biomass as precursors [21,22]. In recent years, biomass materials, such as watermelon peel [23], grapefruit peel [24], corncob [25], bamboo [26,27] seaweed [28], auricularia [29], tea [30] and coconut shell [31], are considered the most important precursor for the preparation of activated carbon [32], owing to low cost, abundant reserves, renewable and environment-friendly.

China is the country with the largest cultivated area and the largest total production of ginger in the world, with an annual output of 12.37 million tons in 2018. But ginger, as an ingredient in food, is discarded after used, resulting in great waste of resources. In this study, porous activated carbon was prepared by carbonizing waste ginger as carbon precursor. The micro-morphology and pore structure of the porous carbon were characterized, and its electrochemical performance in 1M Na_2SO_4 electrolyte was evaluated. The results showed that the porous carbon had good network structure, large surface area, low corrosion resistance, excellent chemical stability and conductivity.

2. Experiment

2.1. Preparation of biomass-based porous carbon

The waste ginger slices were washed with water and put in the oven to dry in 80~100 ℃. Then the dried ginger was ground to powder. The powder was mixed with KOH, urea according to the mass ratio of 2:3:2, then the mixture was stirred evenly with distilled water and dried at 80 ℃. The dried mixture was transferred into a porcelain boat and

placed in a tube furnace to carbonize in Ar for 2 h at 800 ℃ (at 4 ℃ min^{-1} of heating rate). After carbonization, the samples were naturally cooled to room temperature to obtain porous carbon products. The product was washed with 1M HCl until no bubble, then washed with distilled water to neutral, and dried in vacuum oven at 60 ℃, and the porous carbon was obtained. To study the effect of the mass ratio of ginger slice and KOH on the structure of porous carbon, and three mass ratios (1:1, 1:1.5 and 1:2) were selected and the resulting porous carbon materials were labeled as PC_1, $PC_{1.5}$ and PC_2, respectively.

2.2. Structural characterization of porous carbon

The surface morphology of porous carbon was observed by scanning electron microscope (SEM, S-4800, high-tech Company, Japan). The crystal structure of porous carbon material was characterized by X-ray diffraction (XRD, Panaco PANalytical, Netherlands) and laser confocal MicroRaman (Thermal power company, US). The pore structure of carbon was characterized by specific surface area analyzer (BET, Quantachrome, USA).

2.3. Preparation of electrode material and electrochemical performance test

The porous carbon (active material), acetylene black and polyvinylidene fluoride (according to the mass ratio of 8:1:1) were ground evenly in a mortar. Then, the mixture was ground uniformly by adding of DMF, and coated on the nickel mesh (1*1 cm^2, the mass is m_0) to prepare the electrode. The electrode was dried in a vacuum oven at 80 ℃ for 12 h. After dried, the electrode was placed on a tablet press at a pressure of 15 MPa for 15 sec. The weight of the electrode was m_1, and the mass of the active material ($m=m_1-m_0$) in the electrode was obtained. The mass of active material was determined to be approximately 2 mg cm^{-2} on each electrode. 1 M Na_2SO_4 was used as the electrolyte, the saturated calomel electrode and the platinum plate was used as the reference electrode and the counter electrode, respectively. The electrochemical performance was investigated by cyclic voltammetry (CV), galvanostatic charge/discharge (GCD), and electrochemical impedance spectroscopy (EIS) in the three-electrode system. The specific capacitance of the material is determined by the formula (1):

$$C_g = I\Delta t/m\Delta V \quad (1)$$

C is the specific capacitance (F g^{-1}), I and Δt are constant discharge current (A) and discharge time (s), respectively, and m, ΔV are the mass of the electrode active material (g) and the voltage difference (V) in the process of charging and discharging, respectively. Energy density (E) and power density (P) are calculated from Eq. (2) and (3):

$$E=0.5CV^2/3.6 \quad (2)$$

$$P=3600E/\Delta t \quad (3)$$

3. Results and discussion

3.1. Structure and morphology analysis of porous carbon

The SEM images of three porous carbon materials (PC_1, $PC_{1.5}$ and PC_2) were shown in Fig. 1. It can be seen that porous carbon material could be obtained after activation by KOH and urea. The KOH/urea solution is conducive to develop an interconnected pore network structure, which can fabricate micro- and mesopores in the walls of macropores by using the chemical activating agent. However, the structure, the number of holes and the pore size of the porous carbon materials obtained were different with the change of KOH content. It can be seen that from Fig. 1a, when the mass ratio of KOH/ginger slice was 1, the pore size distribution was uneven and in the range of 25 nm-2 um, and the numbers of pores and open pores were not relatively enough, which is not good for rapid diffusion/ transport of electrolyte ions and the improvement of the electrochemical performance of biomass-based carbon. When the mass ratio of KOH/ginger slice was 1.5, a large number of connected pores in $PC_{1.5}$ can be observed in Fig. 1b, and the pore sizes remain unchanged, but the numbers of open pore are much more than in PC_1. So, $PC_{1.5}$ showed higher specific surface area and more adsorption sites, which effectively shortens the transmission path of the ion and increases the speed of ion transport, leading to more excellent rate performance. With the further increasing of KOH content, a part of pores collapses, which is mainly due to the erosion of carbon material caused by the excessive KOH in the activation process. It can be inferred that during the activation process, with the increase of mass ratio of KOH/ginger powder, KOH will gradually erode the carbon material, thus forming a porous structure. With the increase of KOH, the effect of KOH on carbon material was improved, making the pore structure more and more obvious. When there was too much KOH, the excessive erosion reaction would cause the initial pore structure to collapse and block other pores, which is not conducive to the transport of electrolyte ions. The crystal structure of the multistage porous carbon materials (PC_1, $PC_{1.5}$ and PC_2) was determined by XRD, and the results were shown in Fig. 2. In Fig. 2, there was a typical diffraction peak at $2\theta=21°$, which is corresponding to (002) crystal plane of graphite. With the increase of KOH content, the diffraction peak of (002) crystal plane in PC_2 became weaker, indicating that the crystallinity of the (002) crystal plane decreases, leading to decreased specific surface area of the biomass-based porous carbon material. No other diffraction peaks appear in the XRD pattern, indicating that there are no other impurities in the obtained porous carbon material.

Raman spectra of porous carbon materials were shown in Fig. 3. There were two broad peaks at 1346 and 1590 cm^{-1} for PC_1, $PC_{1.5}$ and PC_2, corresponding to the D peak in amorphous carbon or defective graphitized carbon and the G peak in graphitized crystalline carbon. With the increase of KOH, the G and D peak became sharper and sharper, illustrating the improved crystallinity and better graphitization degree in materials. However, when the

amount of KOH was too much (PC_2), the structure of porous carbon material would be damaged and collapsed, thus reducing its electrochemical performance.

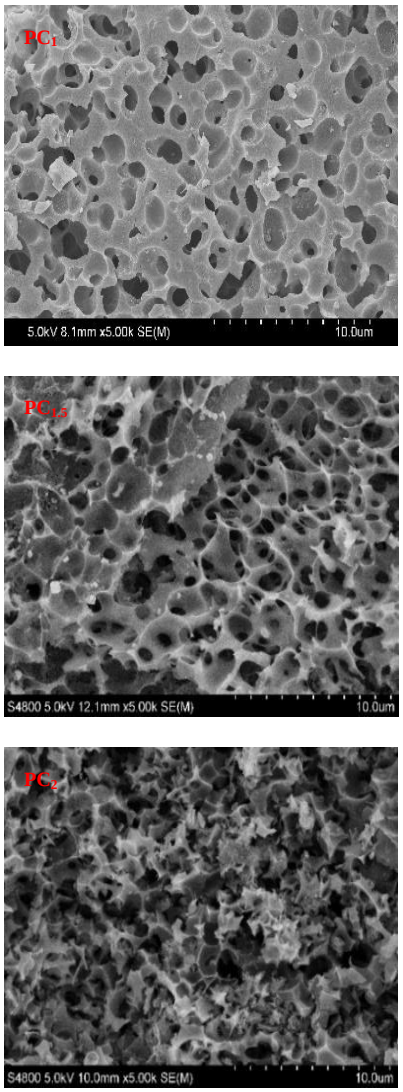

Fig. 1. SEM images of porous carbon materials

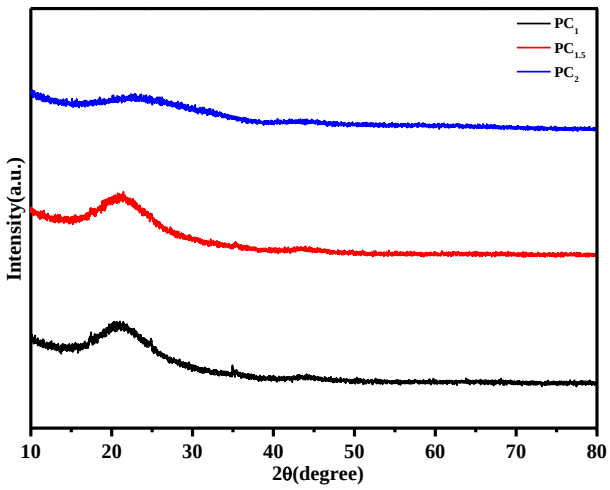

Fig. 2. XRD spectra of porous carbon materials (color online)

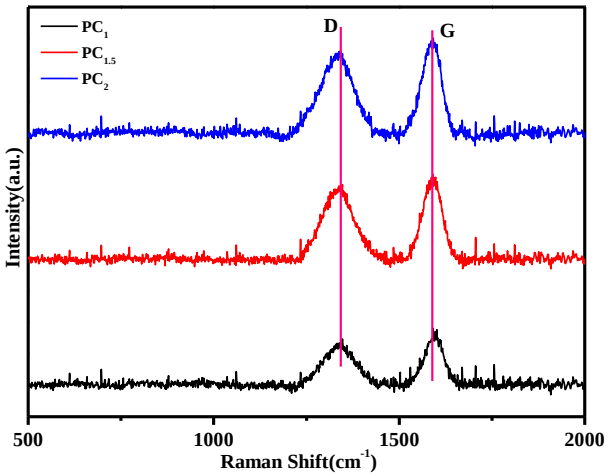

Fig. 3. Raman spectra of porous carbon materials (color online)

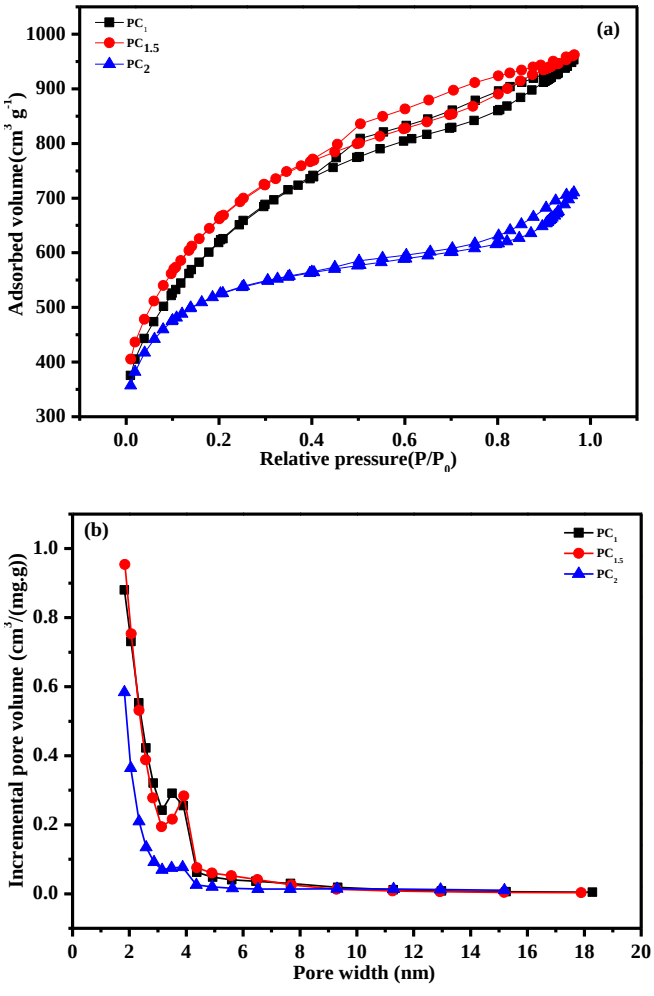

Fig. 4. N_2 sorption isotherms and pore size distributions of porous carbon materials (color online)

In order to further determine the pore structure of the porous carbon, the specific surface area and the pore size distribution were analyzed using the N_2 adsorption and desorption method. As can be seen from Fig. 4a, all porous carbon materials were typical IV adsorption and desorption curves and showed high adsorption capacity, which corresponds to the adsorption behavior of a great number of micro- and mesopores in material. Meanwhile, when the relative pressure was in the range of 0.40-0.90, there were obvious hysteresis rings, corresponding to the porous carbon with mesoporous structure. The pore size distribution obtained according to the non-linear density functional theory model was shown in Fig. 4b, which can also confirm the existence of porous structures such as micro- and mesopores in material. The porous structure can effectively increase the specific surface area of the material, which is beneficial to full contact between active material and electrolyte, effectively increasing the active site. According to the BET specific surface area and the pore size distribution in the adsorption-desorption curve, the porous carbon possessed high specific surface area and appropriate pore size. The specific surface areas of PC_1, $PC_{1.5}$, and PC_2 samples were 2163.64, 2278.63, and 1732 $m^2 g^{-1}$, respectively. Consequently, the specific surface area was highest when the ratio of ginger slices to urea was 1:1.5, and the average pore size of $PC_{1.5}$ was 3.92 nm, which could greatly reduce the ion transmission resistance and diffusion distance, thereby increasing the diffusion/transport speed of electrolyte ions and improving the electrochemical performance of carbon material.

3.2. Electrochemical performance of electrode

The CV curve at a scan rate of 20 mV s^{-1} and the GCD curves at a current density of 1 A g^{-1} for PC_1, $PC_{1.5}$, and PC_2 porous carbon were shown in Fig. 5a and Fig. 5b, respectively. It can be seen from Fig. 5 a-b that at the same scan speed and current density, there were the maximum integrated area in CV curve and the longest charge/discharge time in GCD curves for $PC_{1.5}$, indicating that $PC_{1.5}$ has the largest specific capacitance, which is mainly related to larger specific surface area and more reasonable pore size distribution in 1.5. Furthermore, the $PC_{1.5}$ electrode exhibited higher current density than the others, indicating better electron transportation. The CV curves of $PC_{1.5}$ at different scan rates were shown in Fig. 5c, and all CV curve indicated an approximately rectangular shape and the consistency of these box-like curves at various scan rates, suggesting typical electric double layer capacitance behavior and revealing the excellent capacitive behavior of $PC_{1.5}$ electrode, respectively. The GCD curves of $PC_{1.5}$ electrode at different current densities were shown in Fig. 5d, and there was the largest charge/discharge time when the current density is 0.5 A g^{-1}. This may be due to the fact the electrolyte ions have enough time to enter and diffuse into the pores at a lower current density, so the charge/discharge time decreases significantly with increasing current density. The consistent observation of symmetrical GCD curves at various current densities implied the superior coulombic efficiency and excellent reversibility of $PC_{1.5}$ electrode.

The electrochemical performance of porous carbon materials was further evaluated by EIS and the Nyquist plots of $PC_{1.5}$ electrode was illustrated in Fig. 5e. As can be seen in Fig. 5e, the curves acquired for $PC_{1.5}$ electrode material in 1 M Na_2SO_4 showed a vertical line in the low-medium frequency region, which was characteristic of their capacitive behavior, combined with a semicircle in the high frequency region that can be ascribed to charge transfer processes. The first cut with the X-axis was ascribed to the resistance of the electrolyte (the ion diffusion resistance) and the amplitude of the semicircle was ascribed to the contact resistance of the current collector, intrinsic resistance of the active material and the electron transfer resistance of the electrode material [25]. The sum of all resistances corresponded to the equivalent series resistance (ESR), which was 1.47 Ω. The vertical line in the low-frequency region indicated that the material had good electric double layer capacitance performance, which is attributed to its unique layered porous structure, providing a good channel for the transmission of electrons and electrolytes in the material, thereby greatly reducing the equivalent series resistance, which is beneficial to improve the electrochemical performance of porous carbon electrode. The evaluation of the relation of specific capacitance and current density was performed by charging and discharging $PC_{1.5}$ electrode from 0.5 to 10 A g^{-1} (Fig. 5f). As can be seen that the specific capacitance of $PC_{1.5}$ was a maximum of 227 F g^{-1} at current density of 0.5 A g^{-1}. When the current density increased to 10 A g^{-1}, the capacitance retention was 88%, indicating high specific capacitance and excellent rate performance of carbon electrode ($PC_{1.5}$).

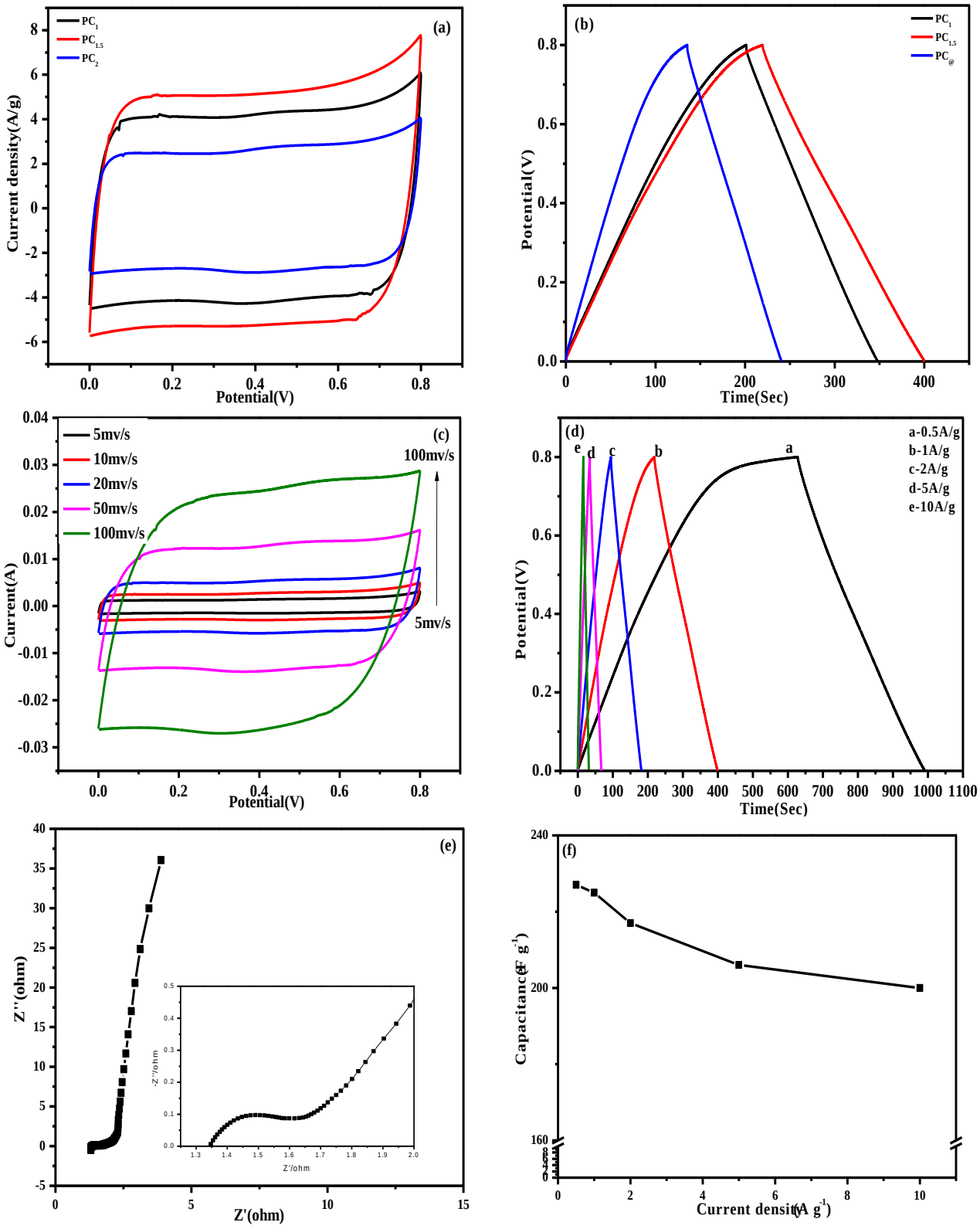

Fig. 5. The electrochemical properties: (a)-CV curves at the scan rate of 20 mV s^{-1} and (b)-GCD curves at the current density of 1 A g^{-1} for PC_1, $PC_{1.5}$ and PC_2 electrode; (c)-CV curves at different scan rates and (d)-GCD curves at different current densities and (e)-Nyquist curve for $PC_{1.5}$ electrode; (f)-Relationship between specific capacitance of $PC_{1.5}$ electrode and current density (color online)

The electrochemical performance of PC_1 electrode was further assessed in a three-electrode system within the potential window of -0.8-0 V. As shown in Fig. 6a, the CV curves exhibited a quasi-rectangular shape, characteristic of

a contribution of EDLC. And the CV curve only showed limited distortion at a high scan rate of 100 mV s^{-1}, indicating a good rate capability of the materials. Fig. 6b showed the GCD curves of PC_1 material at different current densities ranging from 0.5 A g^{-1} to 10 A g^{-1}. All these curves exhibited a quasi-linear shape demonstrating EDLC contribution, consistent with the CV test results. The electrode exhibited a specific capacitance of 213 F g^{-1} at 0.5 A g^{-1}. Fig. 6c showed the Nyquist plot of the electrode materials. It consisted of a semicircle in the high-frequency region and an almost vertical line in the low-frequency region. The almost vertical line in the low-frequency region revealed that EDLC was the dominant capacitance contribution, consistent with both CV and GCD results.

In order to further evaluate the electrochemical performance of carbon materials in practical applications, asymmetric supercapacitor (ASC) was prepared using porous carbon materials in 1M Na_2SO_4 electrolyte. $PC_{1.5}$ was used as the positive electrode, and PC_1 as the negative electrode. In the electrochemical test, the highest voltage can reached 1.6V, which can greatly increase the energy density of the material. This may be attributed to the electrolyte. On account of the thermodynamic stable potential window of water was only 1.23 V. To increase the working voltage of aqueous electrolyte, the most promising approach was to use medium electrolyte (such as Li_2SO_4, Na_2SO_4) and a higher voltage of 1.6-2.0 V could be obtained, which is mainly attributed to low H^+ and OH^- concentration, oxygenated surface functionalities on carbon surface that resulted in high over-potential for HER and OER under the steady state of the electrode.

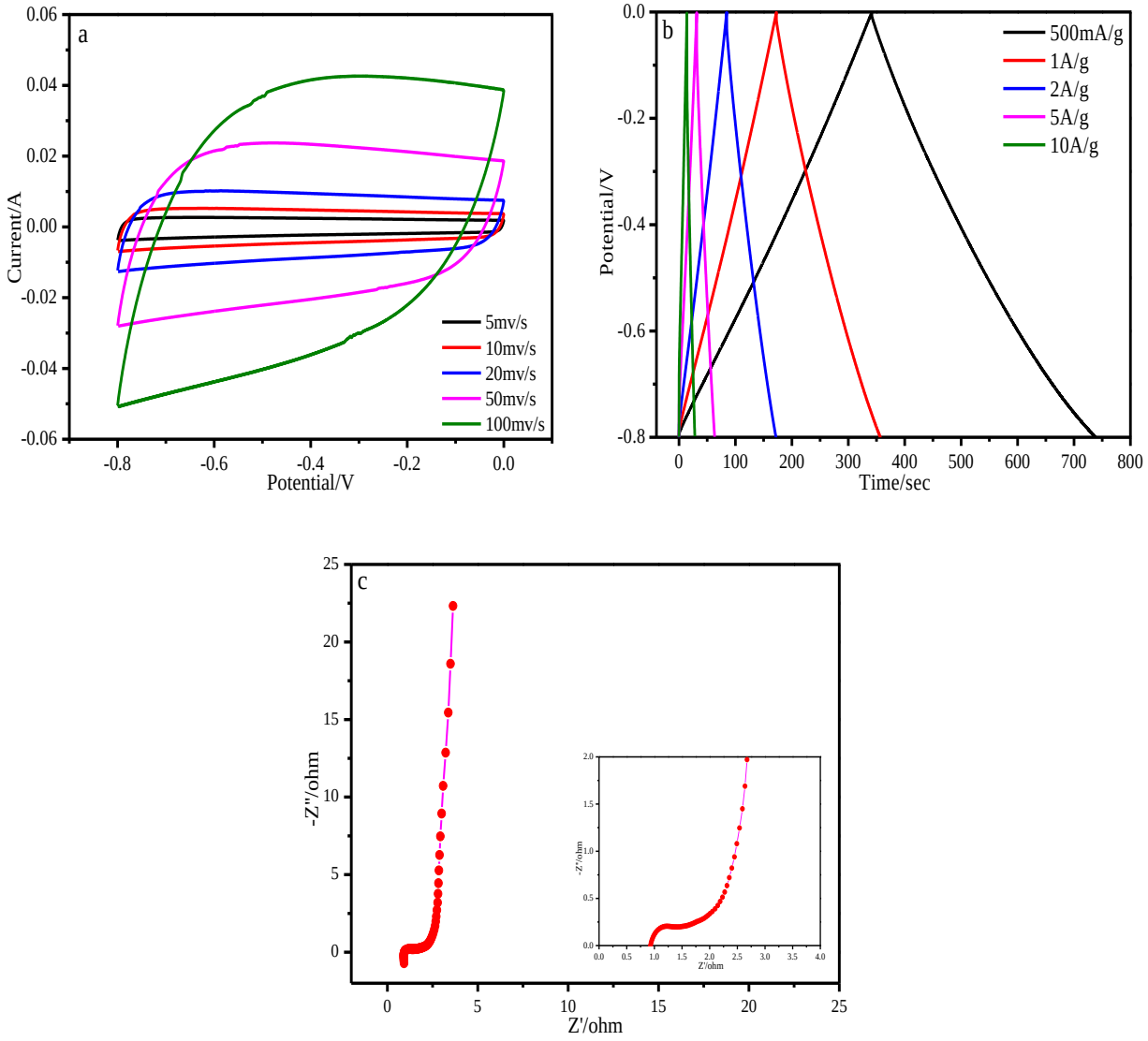

Fig. 6. Electrochemical performance of PC_l in three-electrode system within the potential window of -0.8–0V: (a) CV curves of PC_l at different scan rates from 5 to 100 mV s^{-1}; (b) GCD curves of PC_l at current density from 0.5 to 10 A g^{-1}; (c) Nyquist plots (Inset shows the corresponding magnified plot in the high-frequency region) (color online)

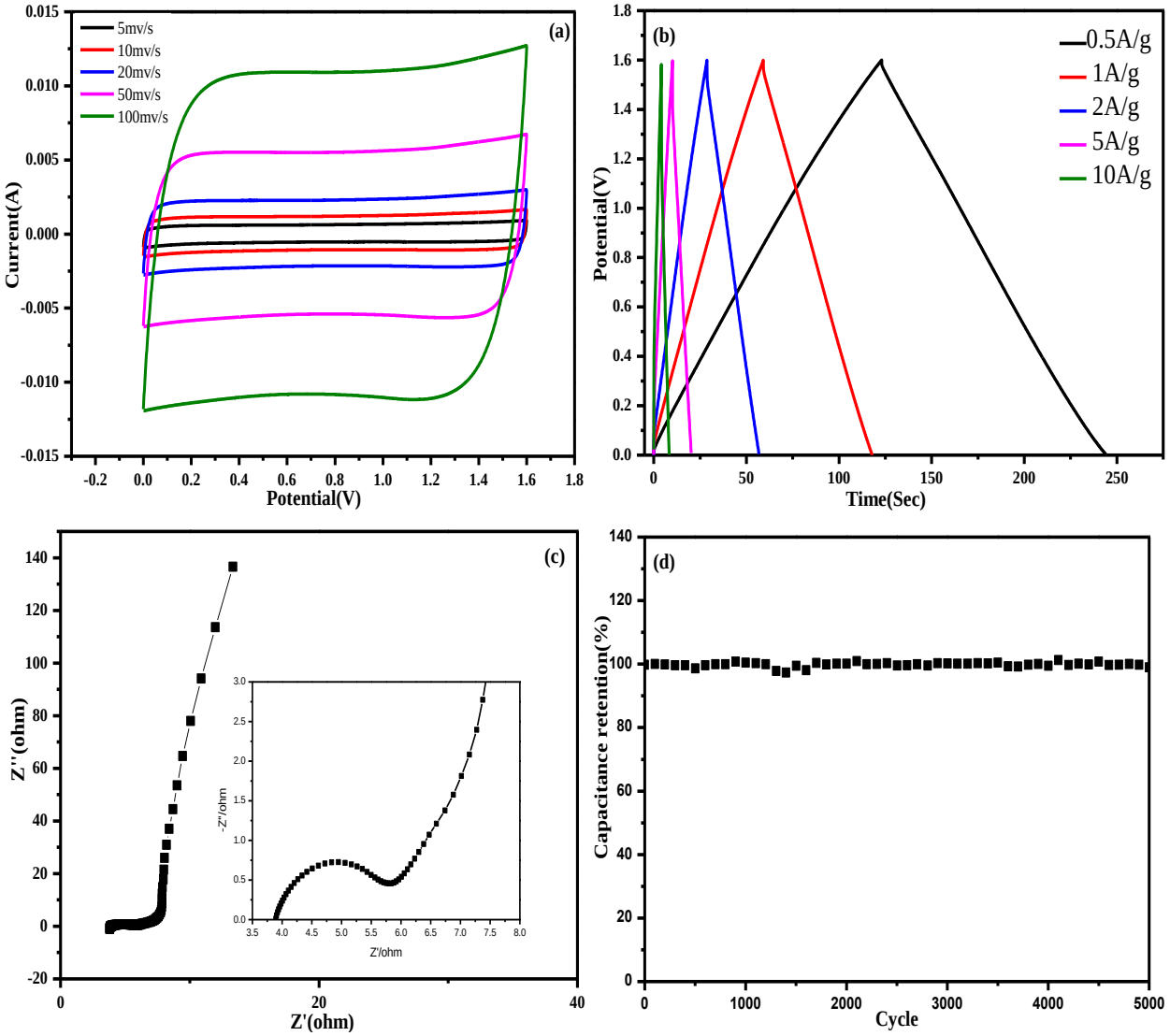

Fig. 7. The electrochemical properties of $PC_{1.5}$//PC_1 system: a-CV curves of $PC_{1.5}$//PC_1 at different scan rates; b-GCD curves of $PC_{1.5}$//PC_1 at different current densities; c-Nyquist curve of $PC_{1.5}$//PC_1; d-Relationship between specific capacitance retention of $PC_{1.5}$//PC_1 and cycling number (color online)

Fig. 7a showed the cyclic voltammetry (CV) curves of the $PC_{1.5}$//PC_1 at different scan rate. All CV curves were approximately rectangular, and no other redox peaks were present, showing typical electric double layer capacitance characteristics. As the scan rate increases, the area of the CV curve increased gradually but still appears rectangular, indicating that the material has good rate performance. Fig. 7b showed the GCD curves of the $PC_{1.5}$//PC_1 at different current density. All the curves were approximately isosceles triangles, indicating that the material has good capacitance and reversibility, and the small voltage drop indicates excellent conductivity.

The impedance test of $PC_{1.5}$//PC_1 ASC was performed in the frequency range of 0.1 Hz to 100 kHz. The EIS diagram of $PC_{1.5}$//PC_1 (shown in Fig.7c) was composed of a semicircle in the high frequency region and a vertical line in the low frequency region. It can be seen from Fig. 6c that in the low frequency region, a line with a larger slope indicated that the prepared porous carbon has good electric double layer capacitance performance, and the diameter of the semicircle in the high frequency region represented the charge transfer resistance (R_{ct}). The R_{ct} was small, which indicated that $PC_{1.5}$//PC_1 had a small contact resistance between the electrolyte and the electrode material, and the ions could move quickly within the connected pore. From the inset in Fig. 6c, it could be clearly observed that the intercept of the X axis of the curve (Rs=3.85 Ω), which represents the equivalent series resistance (R_s) of the carbon electrode, and was related to the resistance of electrolyte, internal resistance of the electrode material, and the contact resistance of between the electrolyte and the electrode material. Fig. 7d showed the specific capacitance retention of $PC_{1.5}$//PC_1 after 5000 times cycles at a current density of

5 A g^{-1}, which was 98.95% of the initial specific capacitance, showing excellent cycling performance.

4. Conclusions

The porous carbon material was prepared using the carbonized material of discarded ginger tablets as a precursor. The synthesized $PC_{1.5}$ material shows good capacitance characteristics in 1M Na_2SO_4 electrolyte: high specific capacitance, better specific capacity retention, excellent rate performance and cycle stability. At a current density of 0.5 A g^{-1}, the specific capacitance is as high as 227 F g^{-1}. Significantly, we have successfully demonstrated a high-performance ASC based on $PC_{1.5}$ anode and PC_1 cathode. $PC_{1.5}$//PC_1 ASC shows an energy density of 13.65 Wh kg^{-1} at a power density of 399.5 W kg^{-1}, especially the capacitance retention is as high as 98.95% after 5000 cycles. The employment of $PC_{1.5}$ anode for ASC broadens the pathway of energy storage devices with high energy and power densities.

Acknowledgments

This research was funded by the Natural Science Foundation of Guangxi Province (2020GXNSFAA159015), Guangxi Key Laboratory of Optical and Electronic Materials and Devices (20KF-20), Innovation Project of Guangxi Graduate Education (JGY2018073), Postgraduate Joint Cultivation Base of the Education Department of Guangxi, Open Funds of Key Laboratory of New Processing Technology for Nonferrous Metal and Materials of Ministry of Education (19AA-18) and Opening Project of Guangxi Key Laboratory of Calcium Carbonate Resources Comprehensive Utilization (Hezhou University) (HZXYKFKT201903).

References

[1] K. Wang, H. Wu, Y. Meng, Z. Wei, Small **10**, 14 (2014).
[2] S. Gong, Z. Jiang, P. Shi, J. Fan, Q. Xu, Y. Min, Appl. Catal. B: Environ. **238**, 318 (2018).
[3] W. Chen, S. Pang, Z. Liu, Z. Yang, X. Fan, D. Fang, J. New Mater. Electr. Sys. **20,** 197 (2017).
[4] X. Li, T. Qian, J. Zai, K. He, Z. Feng, X. Qian, Mater. Today Energy **7**, 10 (2018).
[5] S. Pang, W. Chen, Z. Liu, Z. Yang, X. Fan, X. Xu, J. New Mater. Electr. Sys. **21**, 97(2018).
[6] T. Aida, I. Murayama, K. Yamada, M. Morita, J. Electrochem. Soc. **154**, A798 (2007).
[7] S. Zheng, Z. S. Wu, S. Wang, H. Xiao, F. Zhou, C. Sun, X. Bao, H. Cheng, Energy Storage Mater. **6**, 70 (2017).
[8] B. Fang, L. Binder, Electrochim. Acta **52**, 6916 (2007).
[9] M. Yu, J. Li, L. Wang, Chem. Eng. J. **310**, 300 (2017).
[10] S. Mitra, S.Sampath, Solid State Lett. **7**, A264 (2004).
[11] H. Wang, M. Yoshio, Electrochem. Commun. **8**, 1481 (2006).
[12] E. Gomibuchi, T. Ichikawa, K. Kimura, S. Isobe, K. Nabeta, H. Fujii, Carbon **44**, 983 (2006).
[13] Y. Honda, T. Haramoto, M. Takeshige, H. Shiozaki, T. Kitamura, M. Ishikawa, Electrochem. Solid State Lett. **10**, A106 (2007).
[14] T. Katakabe, T. Kaneko, M. Watanabe, T. Fukushima, T. Aida, J. Electrochem. Soc. **152**, A1913 (2005).
[15] T. Kshetri, D. T. Tran, D.C. Nguyen, N. H. Kim, K. Lau, J. H. Lee, Chem. Eng. J. **380**, 122543 (2020).
[16] B. Xu, F. Wu, S. Chen, C. Zhang, G. Cao, Y. Yang, Electrochim. Acta **52**, 4595 (2007).
[17] Q. Xie, R. Bao, C. Xie, A. Zheng, S. Wu, Y. Zhang, R. Zhang, P. Zhao, J. Power Sources **317**, 133 (2016).
[18] J. Luo, X. Fan, W. Lu, Y. Li, L. Huang, Z. Chen. Polym. Mater. Sci. Eng. **33**, 84 (2017).
[19] Z. Yang, J. Tian, Z. Yin, C. Cui, W. Qian, F. Wei, Carbon **141**, 467 (2019).
[20] W. Zhang, W. Chen, L. Li, S. Pang, X. Fan, Optoelectron. Adv. Mater. **13**, 463 (2019).
[21] Y. P. Zhai, Y. Q. Dou, D. Y. Zhao, P. F. Fulvio, R. T. Mayes, S. Dai, Adv. Mater. **23**, 4828 (2011).
[22] W. Gao, N. Singh, L. Song, Z. Liu, A. L. M. Reddy, L. J. Ci, R. Vajtai, Q. Zhang, B. Q. Wei, P. M. Ajayan, Nat. Nanotechnol. **6**, 496 (2011).
[23] Z. S. Wu, Y. Sun, Y. Z. Tan, S. Yang, X. Feng, K. Müllen, J. Am. Chem. Soc. **134**, 19532 (2012).
[24] H. Jiang, P.S. Lee, C. Li, Energy Environ. Sci. **6**, 41 (2013).
[25] L. Wei, M. Sevilla, A. B. Fuertes, R. Mokaya, G. Yushin, Adv. Func. Mater. **22**, 827 (2012).
[26] F. Zhou, Q. Liu, J. Gu, W. Zhang, D. Zhang, Electrochim. Acta **170**, 328 (2015).
[27] F. Zhou, Q. Liu, D. Kang, J. Gu, W. Zhang, D. Zhang, J. Mater. Chem. A, **2**, 3505 (2014).
[28] D. Kang, Q. Liu, J. Gu, Y. Su, W. Zhang, D. Zhang, ACS Nano **9**, 11225 (2015).
[29] Z. Zhu, H. Jiang, S. Guo, Q. Cheng, Y. Hu, C. Li, Sci. Rep.-UK, **5**, 1 (2015).
[30] C. Peng, X. Yan, R. Wang, J. Lang, J. Ou, Q. Xue, Electrochim. Acta **87**, 401 (2013).
[31] L. Sun, C. Tian, M. Li, X. Meng, L. Wang, R. Wang, J. Yin, H, Fu, J. Mater. Chem. A **1**, 6462 (2013).
[32] Y. W. Zhu, S. Murali, M. D. Stoller, K. J. Ganesh, W. W. Cai, P. J. Ferreira, A. Pirkle, R. M. Wallace, K. A. Cychosz, M. Thommes, D. Su, E. A. Stach, R. S. Ruoff, Science **332**, 1537 (2011).

*Corresponding author: gutming@126.com, xfan@glut.edu.cn